



Cell fate analysis of zone 3 hepatocytes in liver injury and tumorigenesis

Shigeyuki Kurosaki,^{1,†} Hayato Nakagawa,^{1,*} Yuki Hayata,^{1,†} Satoshi Kawamura,¹ Yuki Matsushita,¹ Tomoharu Yamada,¹ Koji Uchino,¹ Yoku Hayakawa,¹ Nobumi Suzuki,¹ Masahiro Hata,¹ Mayo Tsuboi,¹ Hiroto Kinoshita,² Yasuo Tanaka,¹ Takuma Nakatsuka,¹ Yoshihiro Hirata,³ Keisuke Tateishi,¹ Kazuhiko Koike¹

¹Department of Gastroenterology, The University of Tokyo, Tokyo, Japan; ²Division of Gastroenterology, Institute for Adult Diseases, Asahi Life Foundation, Tokyo, Japan; ³Division of Advanced Genome Medicine, The Institute of Medical Science, The University of Tokyo, Tokyo, Japan

JHEP Reports 2021. <https://doi.org/10.1016/j.jhepr.2021.100315>

Background & Aims: Liver lobules are typically subdivided into 3 metabolic zones: zones 1, 2, and 3. However, the contribution of zonal differences in hepatocytes to liver regeneration, as well as to carcinogenic susceptibility, remains unclear.

Methods: We developed a new method for sustained genetic labelling of zone 3 hepatocytes and performed fate tracing to monitor these cells in multiple mouse liver tumour models.

Results: We first examined changes in the zonal distribution of the Wnt target gene *Axin2* over time using *Axin2-Cre^{ERT2};Rosa26-Lox-Stop-Lox-tdTomato* mice (*Axin2;tdTomato*). We found that following tamoxifen administration at 3 weeks of age, approximately one-third of total hepatocytes that correspond to zone 3 were labelled in *Axin2;tdTomato* mice; the *tdTomato*⁺ cell distribution closely matched that of the zone 3 marker CYP2E1. Cell fate analysis revealed that zone 3 hepatocytes maintained their own lineage but rarely proliferated beyond their liver zonation during homeostasis; this indicated that our protocol enabled persistent genetic labelling of zone 3 hepatocytes. Using this system, we found that zone 3 hepatocytes generally had high neoplastic potential, which was promoted by constitutive activation of Wnt/ β -catenin signalling in the pericentral area. However, the frequency of zone 3 hepatocyte-derived tumours varied depending on the regeneration pattern of the liver parenchyma in response to liver injury. Notably, *Axin2*-expressing hepatocytes undergoing chronic liver injury significantly contributed to liver regeneration and possessed high neoplastic potential. Additionally, we revealed that the metabolic phenotypes of liver tumours were acquired during tumorigenesis, irrespective of their spatial origin.

Conclusions: Hepatocytes receiving Wnt/ β -catenin signalling from their microenvironment have high neoplastic potential, and Wnt/ β -catenin signalling is a potential drug target for the prevention of hepatocellular carcinoma.

Lay summary: Lineage tracing revealed that zone 3 hepatocytes residing in the pericentral niche have high neoplastic potential. Under chronic liver injury, hepatocytes receiving Wnt/ β -catenin signalling broadly exist across all hepatic zones and significantly contribute to liver tumorigenesis as well as liver regeneration. Wnt/ β -catenin signalling is a potential drug target for the prevention of hepatocellular carcinoma.

© 2021 The Author(s). Published by Elsevier B.V. on behalf of European Association for the Study of the Liver (EASL). This is an open access article under the CC BY-NC-ND license (<http://creativecommons.org/licenses/by-nc-nd/4.0/>).

Introduction

The liver is composed of small divisions, so-called liver lobules, which consist of a portal triad, linear cords of hepatocytes that are separated by adjacent sinusoids, and a central vein. Liver lobules are typically subdivided into 3 metabolic zones: Zones 1, 2, and 3.^{1–3} Zone 1 hepatocytes encircle portal tracts that are exposed to nutrient- and oxygen-rich blood; they are engaged mainly in glycogen synthesis, gluconeogenesis, protein synthesis, urea synthesis, and β -oxidation of lipids. Zone 3 hepatocytes are

located around the central veins and are responsible for glycolysis, lipogenesis, and biotransformation reactions. Zone 2 hepatocytes are located between zones 1 and 3 and have an intermediate phenotype. In a recent report, single-cell RNA sequencing and single-molecule *in situ* hybridisation (ISH) were applied to demonstrate that liver lobules can be further subdivided into 9 layers based on the expression of zoned landmark genes.⁴ Thus, although hepatocytes appear to be histologically homogenous, they are functionally heterogeneous.

Wnt/ β -catenin signalling plays a pivotal role in determining the function of each hepatic zone.¹ β -catenin signalling is activated in zone 3 pericentral hepatocytes under normal conditions, and inhibition of this pathway prevents pericentral metabolic gene expression in mice.^{5–7} Wnt and R-spondin ligands secreted from central vein endothelial cells maintain activation of Wnt/ β -catenin signalling in zone 3 hepatocytes.^{3,8} Recent cell fate tracing studies in mice have enriched our understanding of

Keywords: Hepatocellular carcinoma; Liver regeneration; Metabolic dysfunction-associated fatty liver disease; Wnt/ β -catenin signal; Metabolic zonation.

Received 14 November 2020; received in revised form 4 May 2021; accepted 7 May 2021; available online 27 May 2021

[†] These authors contributed equally to this work.

* Corresponding author. Address: Department of Gastroenterology, The University of Tokyo, 7-3-1 Bunkyo-ku Hongo, Tokyo 113-8655, Japan. Tel.: +81-3-3815-5411; Fax: +81-3-3814-0021.

E-mail address: hanakagawa-tyk@umin.ac.jp (H. Nakagawa).



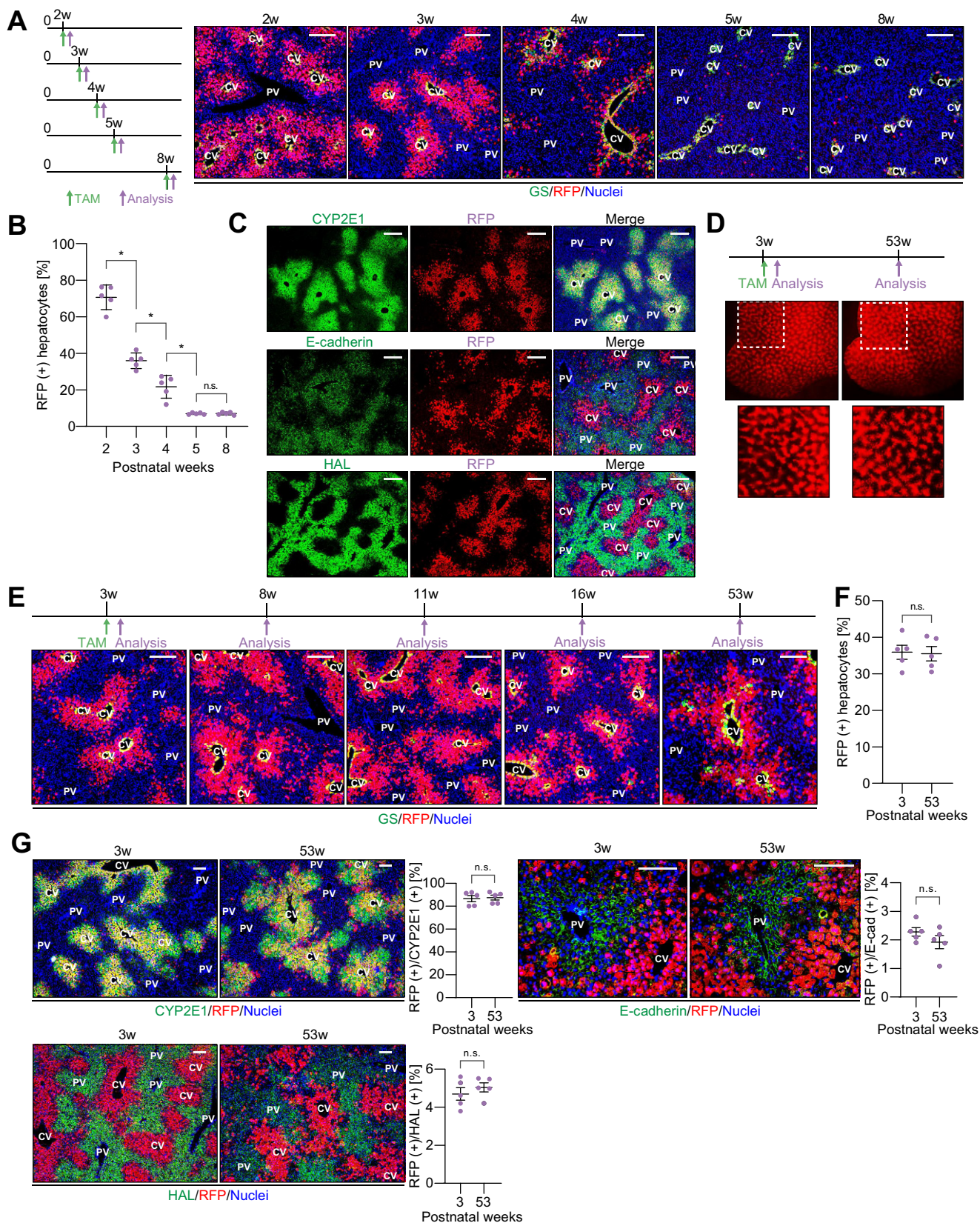


Fig. 1. Development of a persistent genetic labelling system for Zone 3 hepatocytes. (A and B) The distribution of RFP⁺ hepatocytes at 2 days after singular TAM administration. TAM was administered to *Axin2;tdTomato* mice at the indicated ages. Double IF-stained images of the pericentral hepatocyte marker GS (green) and RFP (red) (scale bar: 200 μm) (A). Quantification of the RFP⁺ hepatocytes (**p* < 0.05, Student's *t* test) (B). (C) Double IF-stained images of RFP and indicated proteins in the liver of 3-week-old *Axin2;tdTomato* mice (scale bar: 200 μm). (D–G) Fate tracing at 50 weeks in *Axin2;tdTomato* mouse livers after TAM

tissue homeostasis of the liver. Wang *et al.*⁸ reported that the first few layers of pericentral hepatocytes, as marked by the Wnt target gene *Axin2*, stream from the pericentral to the periportal area and repopulate the majority of hepatocytes during homeostasis, suggesting that pericentral Wnt-receiving hepatocytes act as stem cells in the liver. However, several recent studies have presented evidence against this study and demonstrated that all hepatocytes have similar proliferative potential, regardless of their location.^{6,9–12} Furthermore, 2 very recent studies showed that zone 2 is the region with the highest homeostatic hepatocyte proliferation.^{13,14} Therefore, the mechanism of liver regeneration, including repair responses to liver injury, is still a matter of debate.

The cellular origin of hepatocellular carcinoma (HCC) is another disputed topic. More than 90% of HCCs develop in the context of chronic liver disease.¹⁵ Although hepatitis viral infection is the major cause of HCC at present, metabolic dysfunction-associated fatty liver disease (MAFLD)-based HCC is increasing and is predicted to become the leading cause.¹⁶ Bipotential liver progenitor cells in the biliary compartment proliferate during chronic liver injury and, until recently, were thought to be the origin of HCC. However, recent genetic lineage tracing experiments have suggested that hepatocytes, not biliary cells, are the major cellular source of HCC, even under chronic liver stress.^{17–19} In contrast, the effect of zonal differences on the susceptibility of hepatocytes to carcinogenesis has not yet been elucidated.

Here, we hypothesised that zone 3 hepatocytes have high carcinogenic potential, especially in MAFLD-related hepatocarcinogenesis, because of the following reasons. First, in a previous study, periportal hepatocytes expressing Sox9 did not progress into HCC in several mouse models.¹⁹ Second, pericentral zone 3 hepatocytes are continuously exposed to Wnt/ β -catenin signalling, which is an important driver of HCC development.²⁰ Third, zone 3 hepatocytes abundantly express enzymes involved in xenobiotic detoxification (such as CYP2E1), making them a major site of oxidative stress.²¹ Fourth, zone 3 hepatocytes have the highest rate of lipogenesis and are the main site of lipid accumulation in MAFLD, which results in oxidative DNA damage.²²

Thus, in this study, we developed a new method for sustained genetic labelling of zone 3 hepatocytes and analysed the behaviour and neoplastic potential of these cells using multiple mouse models, with a particular focus on MAFLD-associated liver injury and HCC.

Materials and methods

Animal experiments

Axin2-Cre^{ERT} and *Rosa26-LSL-tdTomato* mice were purchased from the Jackson Laboratory. *MUP-uPA* and *PIK3CA^{T8}* mice were generated as described previously.^{23,24} Wild-type (WT) C57BL/6 mice were purchased from CLEA Japan (Tokyo, Japan). All mice were of the C57BL/6 genetic background. Only male mice were used for the models of liver tumorigenesis. All experiments were approved by the Ethics Committee for Animal Experimentation of the University of Tokyo and the Institute for Adult Diseases,

Asahi Life Foundation. All experiments were conducted according to the Guidelines for the Care and Use of Laboratory Animals.

Histology

Liver tissues were processed for H&E staining and immunostaining as described previously.²⁵ In the case of ISH, perfusion fixation was performed with 4% paraformaldehyde, and *Axin2* mRNA was detected using an RNAscope 2.5 HD Reagent Kit RED (Advanced Cell Diagnostics, Newark, CA, USA).²⁶ Whole-mount fluorescent images and tile scan images were obtained using the MVX100 (Olympus, Tokyo, Japan) and DMI8 (Leica, Wetzlar, Germany) microscopes, respectively. We assessed the expression of red fluorescent protein (RFP) in liver tumours that were larger than 1 mm in diameter. The detailed methods for immunostaining are described in the [Supplementary methods and Table S1](#).

Statistical analyses

Statistical analyses were performed using Student's *t* test or Tukey's multiple comparison test where appropriate. Values of *p* < 0.05 indicate statistical significance. Results are expressed as the mean \pm SEM. All data analyses were performed using GraphPad Prism 8.0 software (GraphPad Software, San Diego, CA, USA).

Additional details are provided in the [Supplementary methods](#).

Results

Development of a persistent genetic labelling system for Zone 3 hepatocytes

The activation of Wnt/ β -catenin signalling in the liver is enhanced during postnatal days 5–20 and then gradually declines with age.²⁷ However, the spatial distribution of Wnt/ β -catenin activation has not yet been explored. Here, we analysed the hepatic zonal distribution of Wnt/ β -catenin activation over time by marking the Wnt target gene *Axin2* using *Axin2-Cre^{ERT2}* mice crossed with *Rosa26-Lox-Stop-Lox-tdTomato* reporter mice (*Axin2;tdTomato*).²⁸ *Axin2;tdTomato* mice aged 2, 3, 4, 5, or 8 weeks were administered tamoxifen (TAM) intraperitoneally, and tdTomato expression was analysed 2 days after TAM administration by immunofluorescence (IF) using anti-RFP antibody. *Axin2⁺* hepatocytes were located around the central veins as reported previously,⁸ but their number changed dramatically with postnatal age (Fig. 1A,B); 70.6% of total hepatocytes were labelled with RFP at 2 weeks of age, after which the RFP⁺ area gradually shrank within the pericentral area. The RFP⁺ cell area plateaued at 5 weeks of age (7.0% of total hepatocytes). ISH analyses using an *Axin2*-specific RNA probe in WT mice also revealed that *Axin2* mRNA was expressed broadly in the pericentral area at 3 weeks of age but was localised in 1 to 2 layers of hepatocytes surrounding the central vein at 5 weeks of age (Fig. S1). Notably, approximately one-third of total hepatocytes (35.9%) were labelled when TAM was administered to 3-week-old mice, and the RFP⁺ distribution pattern coincided with the expression of the typical zone 3

administration at 3 weeks of age. (D) Whole-mount fluorescent images of liver tissue harvested at 2 days and 50 weeks after TAM administration. (E) Double IF-stained images of RFP and GS after the indicated tracing period (scale bar: 200 μ m). (F) Quantification of RFP⁺ hepatocytes at 2 days and 50 weeks after TAM administration (Student's *t* test). (G) Double IF-stained images of RFP and indicated proteins at 2 days and 50 weeks after TAM administration (scale bar: 100 μ m). Scatterplots show the percentage of RFP⁺ hepatocytes (Student's *t* test). CV, central vein; CYP2E1, cytochrome P450 subfamily 2E1; GS, glutamine synthetase; HAL, histidine ammonia lyase; IF, immunofluorescence; n.s., not significant; PV, portal vein; RFP, red fluorescent protein; TAM, tamoxifen.

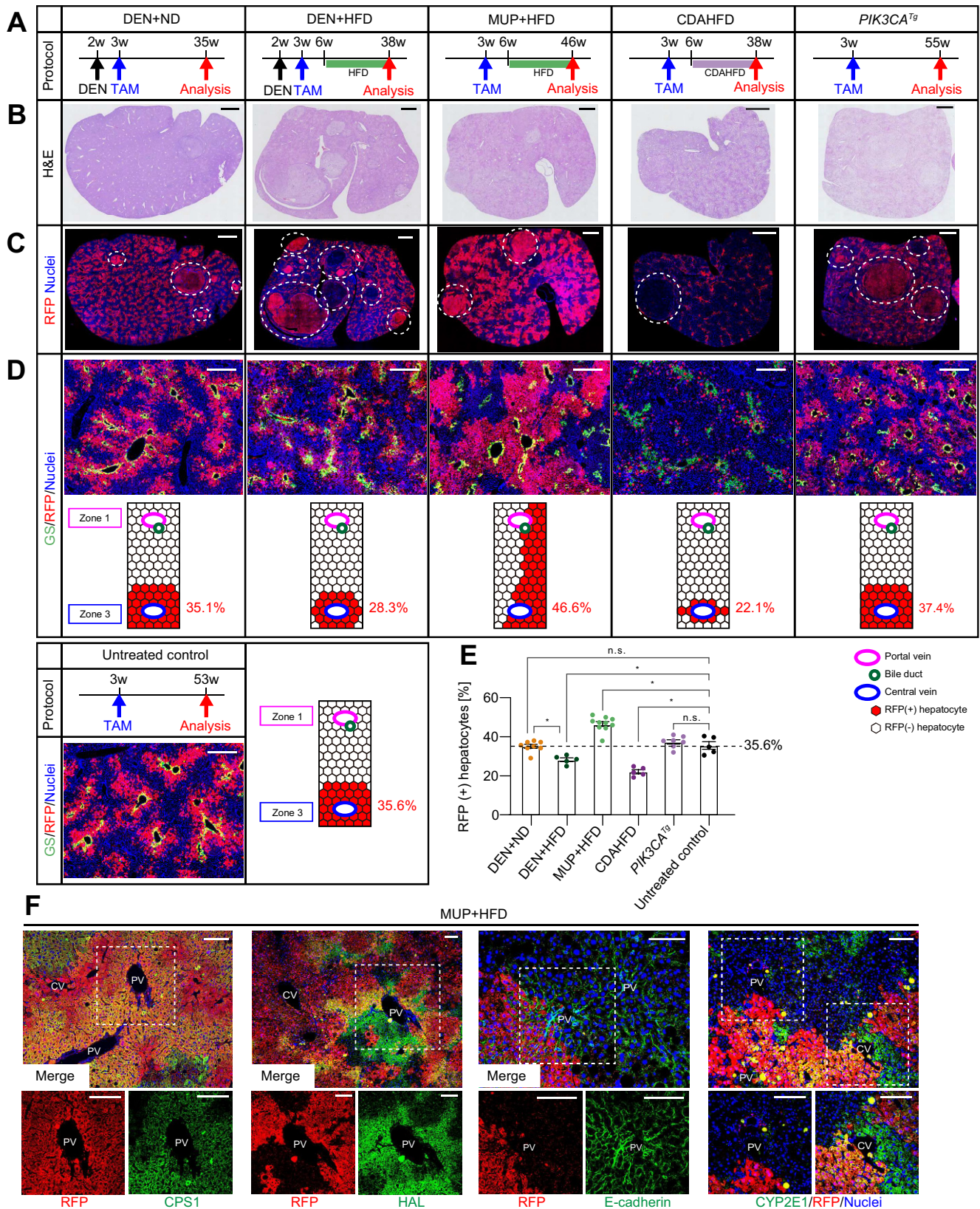


Fig. 2. Fate tracing of Zone 3 hepatocytes. (A) Experimental protocols for each mouse liver tumour model. Representative tile scan images of (B) H&E-stained and (C) RFP-stained liver lobules (scale bar: 2 mm). Dashed lines indicate the liver tumours. (D) Double IF-stained images of RFP and GS of non-tumour areas in each mouse model (scale bar: 500 μ m). Schematic figure showing the distribution of RFP⁺ hepatocytes at the end of each experimental model. An IF-stained image of untreated 53-week-old *Axin2;tdTomato* mice that were administered TAM at 3 weeks of age is also shown for comparison. (E) The percentage of

hepatocyte marker CYP2E1 ($86.7 \pm 2.69\%$ of CYP2E1⁺ hepatocytes). RFP⁺ labelling also presented a mutually exclusive expression pattern with the zone 1 hepatocyte marker E-cadherin ($2.3 \pm 0.1\%$ of E-cadherin⁺ hepatocytes; Fig. 1C). In addition, RFP-expressing hepatocytes rarely expressed histidine ammonia lyase (HAL), a broader periportal marker expressed in zones 1 and 2 ($4.7 \pm 0.3\%$ of HAL⁺ hepatocytes).²⁹ The administration of TAM to 3-week-old *Axin2;tdTomato* mice therefore resulted in the labelling of zone 3 hepatocytes.

Next, we traced the fate of zone 3 hepatocytes labelled in 3-week-old *Axin2;tdTomato* mice. Whole-mount fluorescence analysis revealed clear zonation of RFP expression at 2 days after TAM administration, and this expression pattern was conserved 50 weeks later (Fig. 1D). Similarly, microscopic analysis showed that the distribution and number of RFP⁺ hepatocytes remained almost unchanged during this period, and hepatocytes expressing RFP still mostly co-expressed CYP2E1, but rarely E-cadherin and HAL, at 50 weeks after TAM administration (Fig. 1E–G). These findings indicated that zone 3 hepatocytes maintained their own lineage but rarely proliferated beyond the liver zonation during homeostasis. In other words, this protocol enabled persistent genetic labelling of zone 3 hepatocytes, and we applied this tool to analyse the behaviour of zone 3 hepatocytes under various conditions.

Fate tracing of Zone 3 hepatocytes

To analyse the behaviour and neoplastic potential of zone 3 hepatocytes, we performed fate tracing of zone 3 hepatocytes in 5 mouse models of liver tumorigenesis: diethylnitrosamine (DEN) treatment and feeding with a normal diet (DEN + ND),³⁰ DEN treatment and feeding with a high-fat diet (DEN + HFD),³¹ HFD-fed major urinary protein-urokinase plasminogen activator (*MUP-uPA*) transgenic mice (MUP + HFD),²³ choline-deficient L-amino acid-defined, high-fat diet (CDAHFD) feeding model,³² and hepatocyte-specific transgenic mice harbouring mutant *PIK3CA* variant (*PIK3CA*^{Tg}).²⁴ These are all MAFLD-driven liver tumour models, with the exception of the DEN + ND model.³³ The MUP + HFD and CDAHFD models are steatohepatitis-mediated liver tumour models accompanied by chronic hepatocyte death and compensatory proliferation, whereas *PIK3CA*^{Tg} mice develop hepatic steatosis-based liver tumours without apparent hepatocyte death and inflammation. The experimental protocols for generating each mouse model are shown in Fig. 2A.

We confirmed that the distribution of RFP⁺ hepatocytes in 3-week-old *MUP-uPA;Axin2;tdTomato* and *PIK3CA*^{Tg};*Axin2;tdTomato* mice was similar to that in 3-week-old *Axin2;tdTomato* mice (Fig. S2A). We then showed that DEN administration at 2 weeks of age did not affect the distribution of RFP⁺ hepatocytes in 3-week-old *Axin2;tdTomato* mice (Fig. 2B).

Fig. 2B,C shows the macroscopic appearance and tile scan images of H&E-stained and RFP-stained liver lobes harvested at the end of the experimental protocol for each mouse model. We first analysed the fate of zone 3 hepatocytes in non-tumour liver parenchyma. The number and distribution of RFP⁺ hepatocytes in the DEN + ND model were similar to those in DEN-untreated *Axin2;tdTomato* mice,

whereas in HFD-fed mice, the RFP⁺ area was slightly shifted toward the central vein, and the number of RFP⁺ hepatocytes was lower (28.3%) (Fig. 2D,E). This suggests that HFD feeding promoted regeneration from zone 1/2 hepatocytes. Moreover, in the CDAHFD model, the RFP⁺ area in non-tumour tissues was much smaller (22.1%) and localised near the central vein (Fig. 2D,E). In contrast, in the MUP + HFD model, the number of RFP⁺ hepatocytes in non-tumour areas was increased by 46.6%, and many RFP⁺ hepatocytes had reached the periportal area (Fig. 2C–E). The RFP⁺ hepatocytes that had extended to the periportal area expressed zone 1 hepatocyte marker E-cadherin and periportal metabolic enzymes such as HAL and the urea cycle enzyme carbamoyl phosphate synthetase 1 (CPS1), but not the zone 3 metabolic enzyme cytochrome P450 subfamily 2E1 (CYP2E1; Fig. 2F). This indicates that hepatocytes that had originated from zone 3 were reprogrammed and had gained the functions of zone 1/2 hepatocytes. Conversely, some hepatocytes in the pericentral area had been replaced by RFP⁺ hepatocytes expressing CYP2E1, indicative of bidirectional regeneration in the MUP + HFD model (Fig. 2F). In the *PIK3CA*^{Tg} model, the RFP⁺ area remained largely unchanged 1 year after TAM administration (Fig. 2D,E).

Hepatocytes are largely quiescent during homeostasis but proliferate to replace dead hepatocytes during chronic liver injury, eventually leading to tumour development.¹⁵ Hence, to investigate the differences in liver regeneration patterns between the mouse models, we assessed the zonal location of dying and proliferating hepatocytes in each model. We first analysed the CDAHFD and MUP + HFD models, as these models showed dramatic changes in the number and distribution of RFP⁺ hepatocytes. We used liver samples obtained from 24-week-old mice in each model that revealed a high rate of cell death and compensatory proliferation. As reported previously,²³ apoptotic cells and necrotic cells were stained as nuclear fragmentation and diffuse cytoplasmic pattern, respectively, by terminal deoxynucleotidyl transferase-mediated deoxyuridine triphosphate nick-end labelling (TUNEL) staining in the CDAHFD and MUP + HFD models (Fig. 3A). Dying hepatocytes were abundant in zone 3 in the CDAHFD model, whereas the MUP + HFD model presented a nearly even distribution of dying hepatocytes, with a slightly higher frequency in zones 1 and 2. Ki67⁺ proliferating hepatocytes were more abundant in zones 1 and 2 in the CDAHFD model, whereas the proliferating cells were distributed evenly across all 3 zones with a slightly higher frequency in zone 3 in the MUP + HFD model (Fig. 3A). These findings indicate that the frequency and location of hepatocellular damage determines the regeneration pattern of liver parenchyma (Fig. 3B). We also analysed the DEN + ND, DEN + HFD, and *PIK3CA*^{Tg} models and found that the number of Ki67⁺ proliferating hepatocytes as well as TUNEL⁺ dying hepatocytes was very few, which could result in a relatively stable RFP⁺ area in liver parenchyma (Fig. S3).

Neoplastic potential of Zone 3 hepatocytes

Next, we analysed the neoplastic potential of zone 3 hepatocytes. All tumours that developed in each mouse model were hepatocellular neoplasms, including HCC and hepatocellular adenoma, but not biliary neoplasms (Fig. 4A,B). Assuming that liver

RFP⁺ hepatocytes in non-tumour areas at the end of the experimental protocol (**p* < 0.05, Tukey's multiple comparison test). (F) Double IF-stained images of RFP and indicated proteins in non-tumour tissues of the MUP + HFD model (scale bar: 100 μm). CDAHFD, choline-deficient L-amino acid-defined, high-fat diet; CPS1, carbamoyl phosphate synthetase 1; CV, central vein; CYP2E1, cytochrome P450 subfamily 2E1; DEN, diethylnitrosamine; GS, glutamine synthetase; HAL, histidine ammonia lyase; HFD, high-fat diet; IF, immunofluorescence; MUP, major urinary protein; ND, normal diet; n.s., not significant; *PIK3CA*^{Tg}, hepatocyte-specific transgenic mice harbouring mutant *PIK3CA* variant; PV, portal vein; RFP, red fluorescent protein; TAM, tamoxifen.

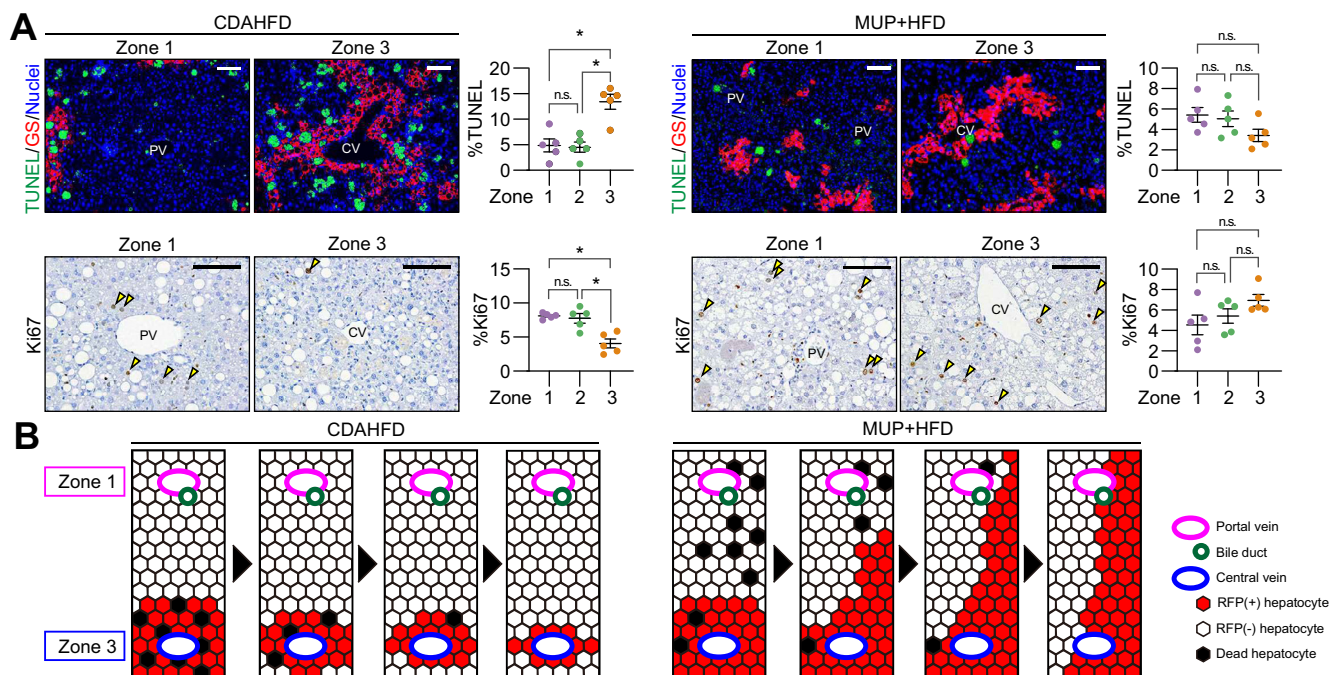


Fig. 3. Zonal location of hepatocyte death affects the regeneration pattern of liver parenchyma. (A) Zonal distribution of TUNEL⁺ dying hepatocytes and Ki67⁺ proliferating hepatocytes of the 24-week-old CDAHFD and MUP + HFD models. Upper panels show double IF-stained images of TUNEL and GS, and lower panels show immunohistochemical images of Ki67 (scale bar: 100 μm). Yellow arrowheads, Ki67⁺ hepatocytes. Scatterplots show the percentage of TUNEL⁺ or Ki67⁺ hepatocytes in each zone (**p* < 0.05, Student's *t* test). (B) Schematic figure showing the behaviour of RFP⁺ hepatocytes. CDAHFD, choline-deficient L-lysine, methionine-deficient, high-fat diet; CV, central vein; GS, glutamine synthetase; HFD, high-fat diet; IF, immunofluorescence; MUP, major urinary protein; n.s., not significant; RFP, red fluorescent protein; TUNEL, terminal deoxynucleotidyl transferase-mediated deoxyuridine triphosphate nick-end labelling; PV, portal vein.

tumours arise uniformly from all hepatic zones, the frequency of RFP-expressing liver tumours was expected to be approximately 35% in all mouse models, which was calculated from the initial RFP positive rate of hepatocytes. Of the DEN-initiated liver tumour models, the rate of RFP-expressing tumours was 80.7% for the DEN + ND model and 55.8% for the DEN + HFD model, both of which exhibited higher RFP expression rates than initially estimated (Fig. 4C,D). As DEN is mainly considered to be metabolically activated in zone 3 hepatocytes expressing CYP2E1,³⁴ these results were reasonable and indicated the validity of this experimental system. High frequencies of RFP⁺ tumours were also observed in the MUP + HFD model (67.0%) and *PIK3CA*^{Tg} model (67.6%), which were approximately twice as high as estimated. By contrast, only the CDAHFD model presented a lower than expected rate of RFP⁺ tumours (25.0%) (Fig. 4D). Zone 3 hepatocytes therefore possessed higher neoplastic potential than estimated initially, except for those in the CDAHFD model.

Importantly, the frequency of RFP⁺ tumours generally corresponded to the changes of the RFP⁺ hepatocytes in non-tumour areas across all mouse models (Figs. 2D and 4D). A typical example is the CDAHFD model, which displayed the lowest frequency of RFP⁺ tumours as well as significant regeneration from zone 1/2 hepatocytes. Furthermore, contrary to our expectations, the frequency of RFP⁺ tumours in the DEN model was relatively low in HFD-fed mice, despite the significantly higher number of liver tumours (Fig. 4E). The number of RFP⁺ tumours was comparable between the DEN + ND and DEN + HFD models, whereas the number of RFP⁻ tumours was significantly higher in HFD-fed mice (Fig. 4E); this suggests that HFD feeding promoted zone 1/2 hepatocyte-derived tumour development along with liver

regeneration from zone 1/2 hepatocyte. Taken together, although zone 3 hepatocytes generally possess high neoplastic potential, the frequency of zone 3 hepatocyte-derived tumours varied depending on the regeneration pattern of liver parenchyma (Fig. 4F).

Inhibition of the pericentral Wnt/β-catenin-activating niche suppresses DEN-induced hepatocarcinogenesis

β-Catenin mutation is often observed during early hepatocarcinogenesis in humans, and activation of Wnt/β-catenin signalling is involved in maintaining HCC-initiating cells.^{35,36} However, mouse HCCs induced by DEN do not show mutation and/or activation of Wnt/β-catenin pathway components.³⁷ Consistent with this finding, expression of glutamine synthetase (GS), a surrogate β-catenin target, was not present in DEN-induced HCC tissues developed in *Axin2;tdTomato* mice at 8 months of age, irrespective of RFP expression (Fig. 5A). Interestingly, premalignant foci located in the pericentral area often expressed GS and RFP in 5-month-old DEN-injected *Axin2;tdTomato* mice (Fig. 5A). Based on these findings, we hypothesised that pericentral activation of Wnt/β-catenin signalling in zone 3 might provide a niche in which tumour-initiating cells can survive and grow during early hepatocarcinogenesis. To test this hypothesis, we treated DEN-injected WT mice with porcupine inhibitor LGK974, which inhibits palmitoylation and secretion of Wnt family proteins. First, we demonstrated that expression of *tdTomato* as well as *Axin2* mRNA was significantly lower in 5-week-old *Axin2;tdTomato* mouse livers following LGK974 administration, which indicated efficient inhibition of Wnt/β-catenin signalling (Fig. 5B). Next, we injected 2-week-old WT mice with DEN and then treated the mice with LGK974 or vehicle control for

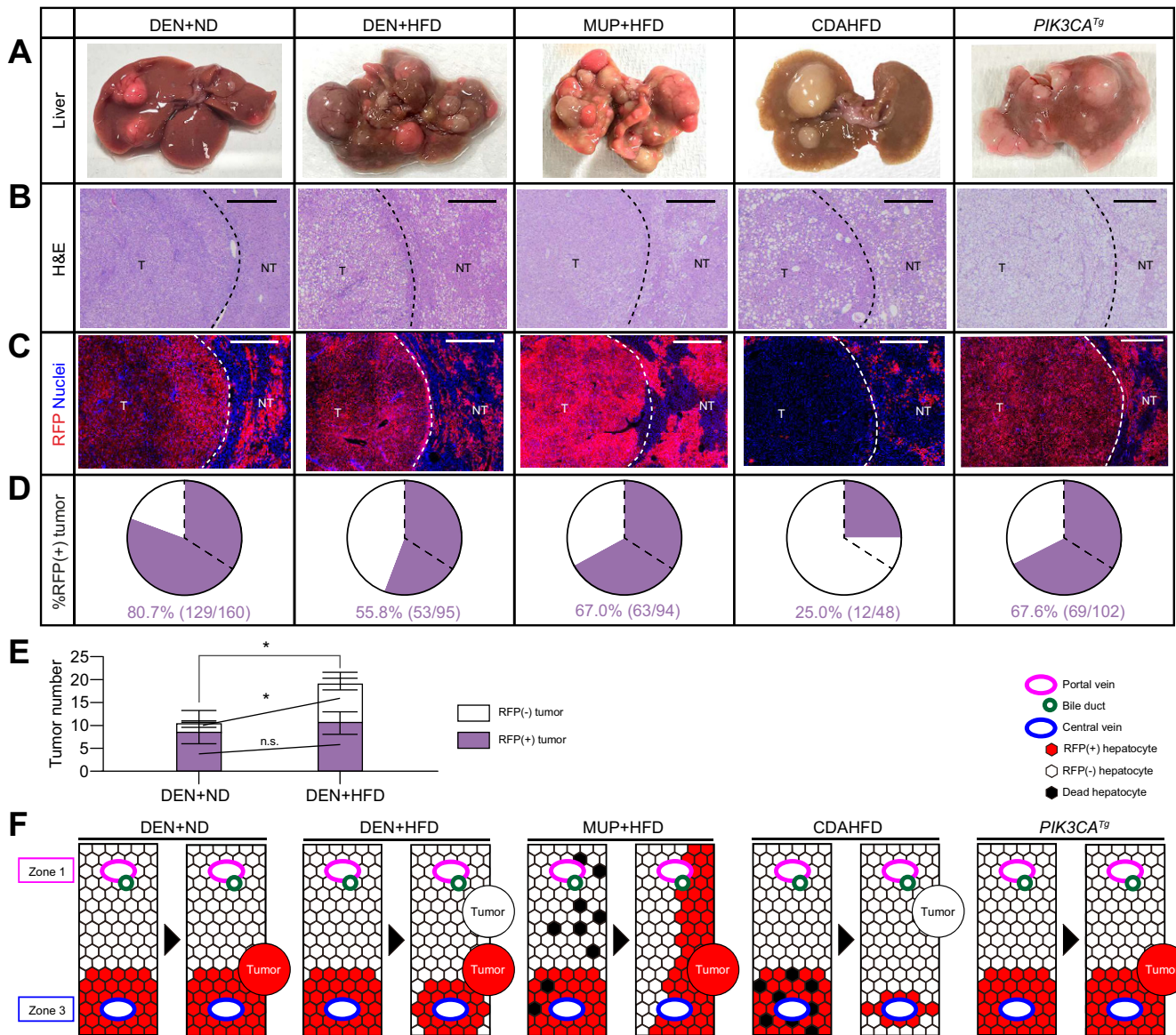


Fig. 4. The neoplastic potential of Zone 3 hepatocytes. (A) Representative macroscopic images of liver tissue from each mouse model. Representative images of (B) H&E-stained and (C) RFP-stained liver tissues (scale bar: 500 μ m). (D) Pie charts showing the percentage of RFP⁺ liver tumours in each mouse model (liver analysed: DEN + ND, n = 8; DEN + HFD, n = 5; MUP + HFD, n = 10; CDAHFD, n = 5; *PIK3CA*^{Tg}, n = 7). The numbers of analysed tumours are also shown under the pie charts. Dashed lines in pie charts represent the estimated frequency of RFP⁺ tumour. (E) Tumour numbers in the DEN + ND and DEN + HFD models were analysed separately for RFP expression (DEN + ND, n = 8; DEN + HFD, n = 5); **p* < 0.05 (Student's *t* test). (F) Schematic figure showing neoplastic potential of RFP⁺ cells and its correlation with liver regeneration pattern in each mouse model. CHAHFD, choline-deficient L-amino acid-defined, high-fat diet; DEN, diethylnitrosamine; HFD, high-fat diet; MUP, major urinary protein; ND, normal diet; n.s., not significant; NT, non-tumour; *PIK3CA*^{Tg}, hepatocyte-specific transgenic mice harbouring mutant *PIK3CA* variant; RFP, red fluorescent protein; T, tumour.

a 3-month period at ages 2–5 months; this period is considered the promotion phase of DEN-induced hepatocarcinogenesis. We also treated DEN-injected *Axin2*;*tdTomato* mice with LGK974 and confirmed the decreased GS expression in pericentral premalignant foci at 5 months of age (Fig. 5C). Then we analysed tumour development at 8 months after DEN injection. As shown in Fig. 5D,E, the HCC incidence rate and tumour growth were significantly reduced in mice treated with LGK974. These findings suggest that a pericentral Wnt/ β -catenin-activating niche may promote HCC development in zone 3 hepatocytes.

Axin2-expressing hepatocytes subjected to chronic liver injury contribute to liver regeneration but possess high neoplastic potential

Next, we explored the role of Axin2-expressing hepatocytes during chronic liver injury. *MUP-uPA* mice undergo transient liver injury that starts at approximately 4 weeks of age and resolves by 13 weeks.³⁸ However, subjecting *MUP-uPA* mice to a HFD from 6 weeks of age induced steatohepatitis and sustained hepatocyte death, which results in compensatory hepatocyte proliferation and HCC development.²³ Thus, we began by

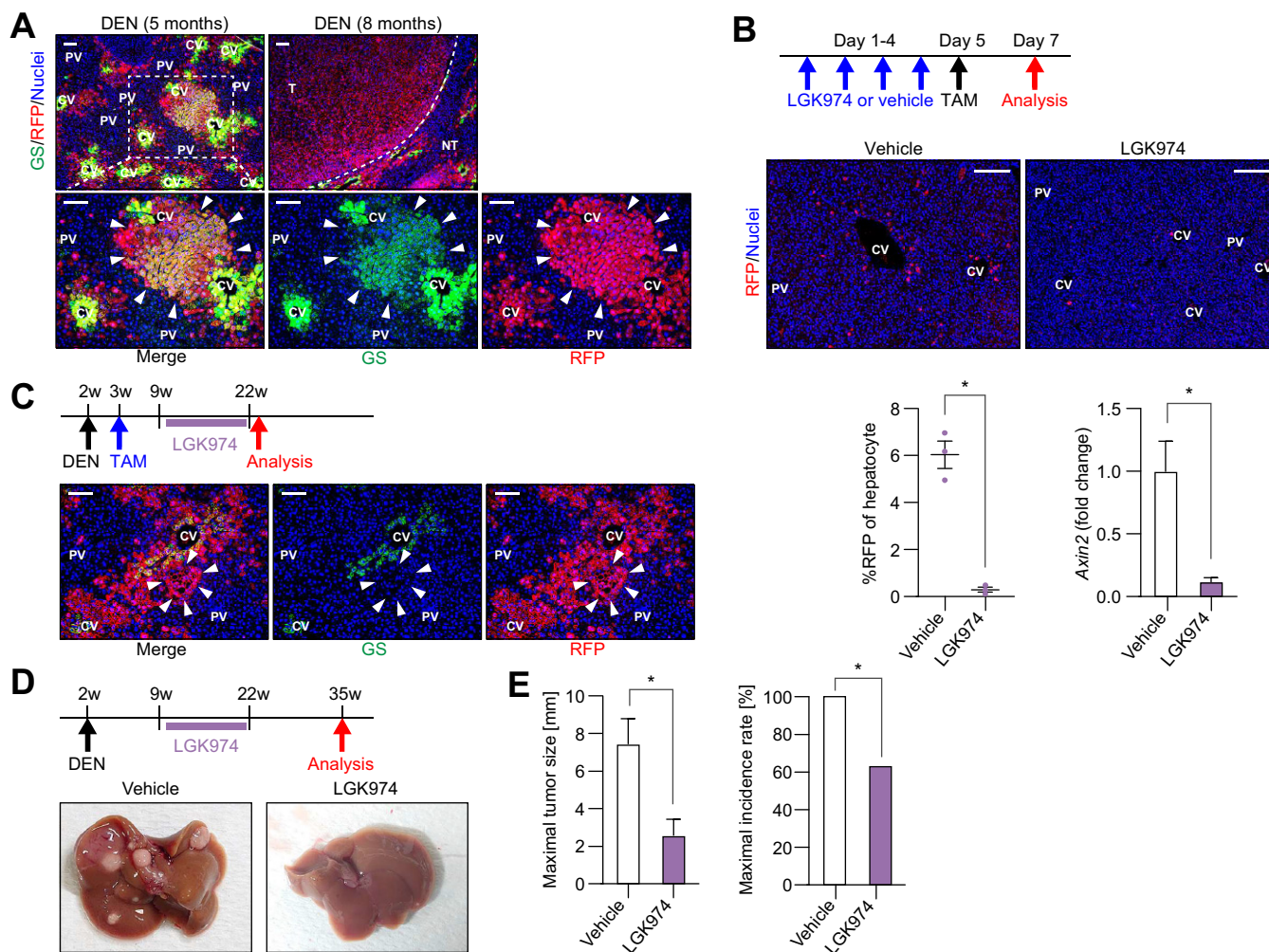


Fig. 5. Inhibition of the pericentral Wnt/ β -catenin-activating niche suppresses DEN-induced hepatocarcinogenesis. (A) Double IF-stained images of RFP and GS in DEN-induced premalignant foci and HCC in *Axin2;tdTomato* mice (scale bar: 100 μ m). Images of premalignant foci and HCC are obtained from 5-month-old and 8-month-old DEN-injected *Axin2;tdTomato* mice, respectively. White arrowheads, premalignant foci. (B) IF-stained images of RFP in vehicle- or LGK974-treated 5-week-old *Axin2;tdTomato* mice (scale bar: 200 μ m). LGK974 was given as depicted in the experimental protocol. Lower left panel, percentage of RFP⁺ hepatocytes; lower right panel, hepatic expression levels of *Axin2* mRNA determined by real-time PCR, (n = 3 per group); *p < 0.05 (Student's *t* test). (C) Double IF-stained image of RFP and GS in premalignant foci of DEN-injected 5-month-old *Axin2;tdTomato* mice treated by LGK974 (scale bar: 100 μ m). (D and E) LGK974 treatment suppresses DEN-induced HCC development. (D) Protocol for LGK974 treatment and representative macroscopic images of the liver in vehicle- or LGK974-treated mice. (E) Bar graphs show tumour incidence rate and maximal tumour size (n = 11 per group); *p < 0.05 (Student's *t* test). CV, central vein; DEN, diethylnitrosamine; GS, glutamine synthetase; HCC, hepatocellular carcinoma; IF, immunofluorescence; NT, non-tumour; PV, portal vein; RFP, red fluorescent protein; T, tumour; TAM, tamoxifen.

examining *Axin2* expression in 5-week-old *MUP-uPA;Axin2;tdTomato* mice experiencing liver injury (Fig. 6A). The number of RFP⁺ hepatocytes was significantly higher in *MUP-uPA;Axin2;tdTomato* mice than in *Axin2;tdTomato* mice at age 5 weeks, and RFP⁺ hepatocytes of *MUP-uPA;Axin2;tdTomato* mice were not restricted to zone 3 but were scattered across all 3 hepatic zones and sometimes expressed HAL and E-cadherin (Fig. 6B and Fig. S4). Such a distribution of *Axin2*-expressing cells was confirmed by ISH analysis of *Axin2* mRNA (Fig. 6C). Interestingly, the frequency of Ki67 expression in RFP⁺ cells was significantly higher than that in RFP⁻ cells (Fig. 6D). To evaluate the contribution of these *Axin2*-expressing hepatocytes to liver regeneration and tumorigenesis, we labelled *Axin2*⁺ cells in *MUP-uPA;Axin2;tdTomato* mice at 5 weeks of age and began HFD

feeding at 6 weeks; we then analysed RFP expression at 46 weeks of age (Fig. 6E). Notably, whole-mount fluorescence analysis revealed that most liver tissues, as well as liver tumours, expressed *tdTomato* (Fig. 6E). Histological analyses showed that 86.5% of the liver tumours (90/104; liver analysed, n = 8) were positive for RFP, and 88.7 ± 1.3% of hepatocytes in non-tumour liver parenchyma were replaced with RFP⁺ cells (Fig. 6F). By contrast, under normal conditions, RFP⁺ cells labelled at 5 weeks of age in *Axin2;tdTomato* mice revealed only slight expansion at 46 weeks of age (5 weeks, 6.9 ± 0.3%; 46 weeks, 8.3 ± 0.6%; p = 0.01). These findings indicated that *Axin2*-expressing hepatocytes subjected to chronic liver injury significantly contributed to liver regeneration and possessed high neoplastic potential (Fig. 6G).

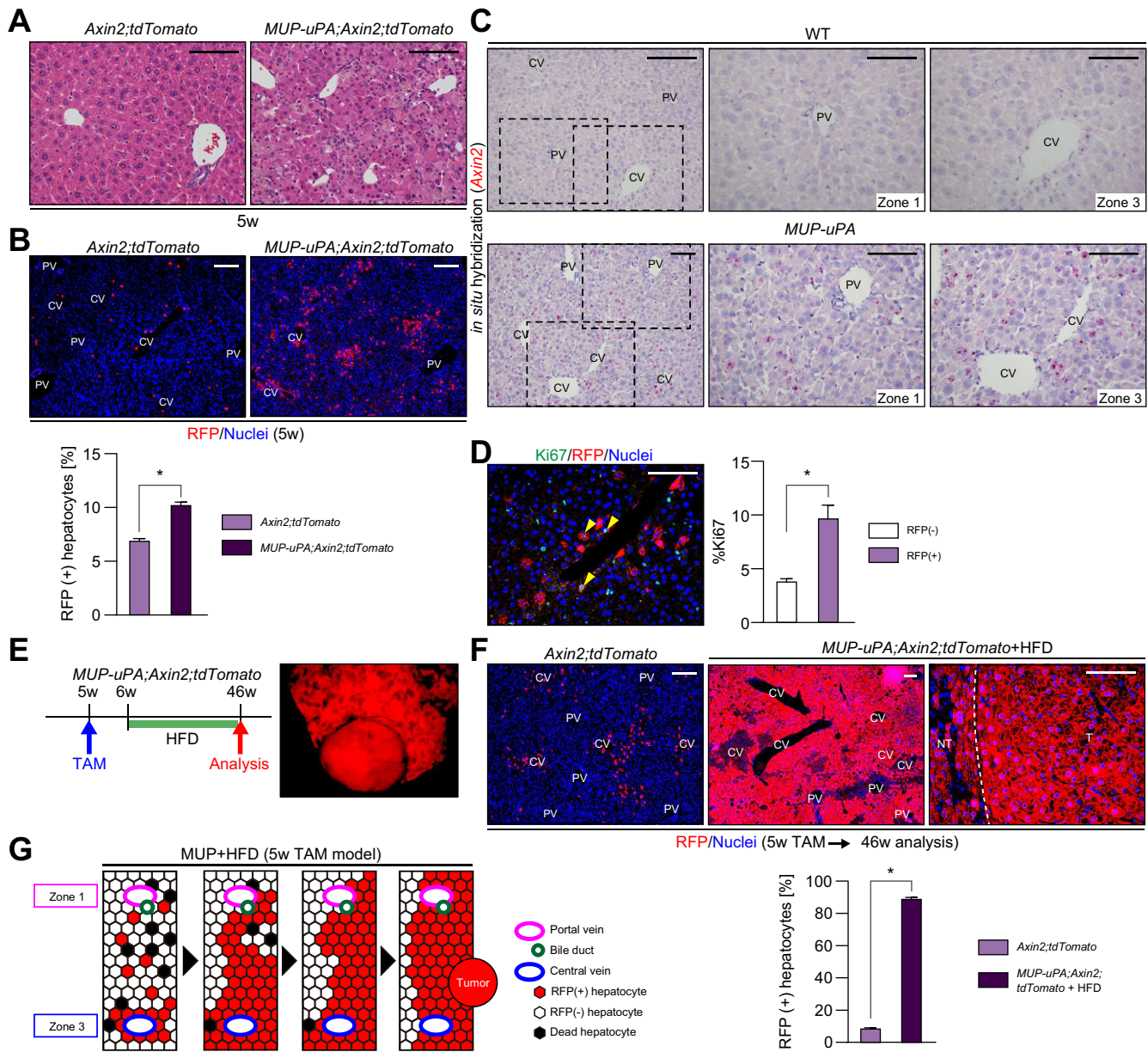


Fig. 6. Fate tracing of Axin2-expressing hepatocytes under chronic liver injury. (A) H&E-stained images of the liver from 5-week-old WT and *MUP-uPA* mice (scale bar: 100 μ m). (B) RFP expression in 5-week-old *Axin2;tdTomato* and *MUP-uPA;Axin2;tdTomato* mice at 2 days after TAM administration (scale bar: 200 μ m). Bar graph shows the percentage of RFP⁺ hepatocytes (*Axin2;tdTomato*, n = 4; *MUP-uPA;Axin2;tdTomato*, n = 3); **p* < 0.05 (Student's *t* test). (C) ISH images of *Axin2* in the liver from 5-week-old WT and *MUP-uPA* mice (scale bar: 50 μ m). (D) Double IF-stained images of Ki67 and RFP in 5-week-old *Axin2;tdTomato* and *MUP-uPA;Axin2;tdTomato* mice at 2 days after TAM administration (scale bar: 100 μ m). Yellow arrowheads, Ki67⁺/RFP⁺ hepatocytes. Bar graph shows the frequency of Ki67⁺ hepatocytes in RFP⁺ or RFP⁻ hepatocytes (n = 3); **p* < 0.05 (Student's *t* test). (E) Experimental protocol for cell fate tracing of Axin2-expressing cells subjected to chronic liver injury. Photograph shows whole-mount fluorescent image of liver tissue at the end of the experimental protocol. (F) IF staining of RFP in *Axin2;tdTomato* mice and HFD-fed *MUP-uPA;Axin2;tdTomato* mice at the end of the experimental protocol (scale bar: 100 μ m). Bar graph shows the percentage of RFP⁺ hepatocytes (*Axin2;tdTomato*, n = 3; *MUP-uPA;Axin2;tdTomato*, n = 8); **p* < 0.05 (Student's *t* test). (G) Schematic figure showing expansion and neoplastic potential of Axin2⁺ cells during chronic liver injury. CV, central vein; HFD, high-fat diet; IF, immunofluorescence; ISH, *in situ* hybridisation; MUP, major urinary protein; NT, non-tumour; PV, portal vein; RFP, red fluorescent protein; T, tumour; TAM, tamoxifen; WT, wild type.

Spatial origin does not determine the metabolic phenotype of liver tumours

A recent study identified 2 well-differentiated subclasses of HCC, named 'perivenous (PV)-type HCC' and 'periportal (PP)-type HCC', according to where their phenotypes lie on the metabolic zonation spectrum.²⁹ However, it is still unclear whether the metabolic

phenotypes of HCC tumours are inherited from their spatial origin or acquired during tumorigenesis. To address this, we compared the expression of various zonation markers between RFP⁺ (perivenular hepatocyte-derived) and RFP⁻ (periportal hepatocyte-derived) tumours. As shown in Fig. 7, the PV-type HCC marker GS

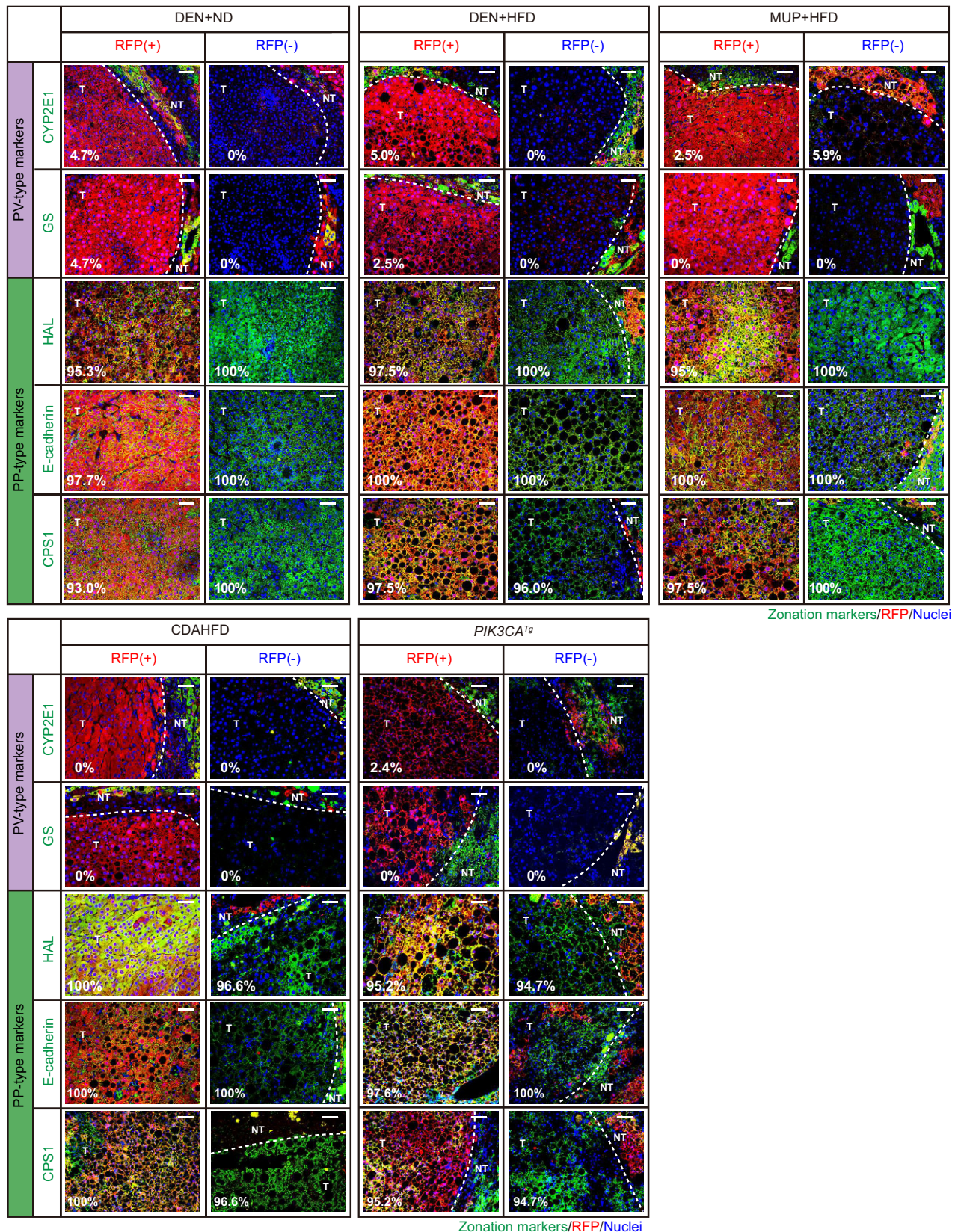


Fig. 7. Spatial origin does not determine the metabolic phenotype of liver tumours. Double IF-stained images of RFP (red) and GS, CYP2E1 (pericentral markers), E-cadherin, CPS1, or HAL (periportal markers) (green) in the tumour tissues of each mouse model (scale bar: 50 µm). Percentages of the tumours expressing each marker are also shown. CDAHFD, choline-deficient L-amino acid-defined; CPS1, carbamoyl phosphate synthetase 1; CYP2E1, cytochrome P450 subfamily 2E1; DEN, diethylnitrosamine; GS, glutamine synthetase; HAL, histidine ammonia lyase; HFD, high-fat diet; IF, immunofluorescence; MUP, major urinary protein; ND, normal diet; NT, non-tumour; PP, periportal; PV, perivenous; RFP, red fluorescent protein; T, tumour.

was expressed in relatively few tumours in our 5 mouse models. Another PV-type HCC marker, CYP2E1, was not expressed at all, even in RFP⁺ tumour cells that had originally expressed CYP2E1 before developing into tumours. The PP-type HCC markers E-cadherin, CPS1, and HAL were expressed in most tumour cells, regardless of RFP expression (Fig. 7). These findings indicate that the liver tumours developed in this study were mostly the PP-type metabolic phenotype regardless of their spatial origin and that their phenotypes were acquired during tumorigenesis.

Discussion

Very few studies, so far, have investigated the zonal location of the cellular origin of HCC. Font-Burgada *et al.*¹⁹ genetically labelled 1 to 2 layers of periportal Sox9⁺ hepatocytes (accounting for 2.9% of total hepatocytes) and showed that the Sox9⁺ periportal hepatocytes did not give rise to HCC. During the preparation of this manuscript, Ang *et al.*³⁹ genetically labelled a few layers of pericentral LGR5⁺ hepatocytes (accounting for 2% of total hepatocytes) and showed that approximately 40% of DEN-induced HCCs were derived from LGR5⁺ pericentral hepatocytes. They also showed that induction of active Her2 mutation in LGR5⁺ pericentral hepatocytes promoted HCC development. These findings suggest that pericentral hepatocytes may be more susceptible to neoplastic transformation than periportal hepatocytes. However, because these studies marked small percentages of the total hepatocyte population, they were not able to elucidate completely the zonal differences in neoplastic potential within the liver. In this study, we labelled zone 3 hepatocytes, which accounted for approximately one-third of total hepatocytes, making it possible to compare the neoplastic potential of hepatocytes depending on their zonal location.

An advantage of our study is that we used various types of liver tumour mouse models, including chemical carcinogen models, chronic liver injury models, and a transgenic mouse model that lacks cell death and inflammation. The *PIK3CA*^{Tg} model enables the simplest comparison of the neoplastic potential between pericentral and periportal hepatocytes, because the RFP⁺ areas in non-tumour liver tissue were almost unchanged during the observation period in this model. Nevertheless, approximately two-thirds of liver tumours expressed RFP, indicative of the high neoplastic potential of zone 3 hepatocytes. Furthermore, inhibition of Wnt/β-catenin signalling significantly reduced HCC development in the DEN + ND model, in which Wnt/β-catenin signalling was no longer activated in developed tumours. This suggests that a Wnt/β-catenin-activating niche may be responsible for the early stages of hepatocarcinogenesis in zone 3 hepatocytes. Therefore, Wnt/β-catenin signalling is considered a drug target for the prevention of HCC.

Contrary to our expectations, tumorigenesis of zone 1/2 hepatocytes was promoted in DEN-injected mice fed the HFD. DEN is preferentially metabolised and activated by zone 3 hepatocytes.³⁴ It is possible that a small amount of DEN was also metabolised in zone 2, but the DNA damage was not sufficient to cause tumour development under ND conditions. Typically, HFD triggers mild cell death in zone 3, and regenerative responses in zone 1/2 hepatocytes; this can promote tumorigenesis in zone 2 hepatocytes that have suffered mild DNA damage. Although we could not detect apparent cell death in the DEN + HFD model probably as a result of low frequency of dying hepatocytes, the

findings obtained from CDAHFD model supported this notion. CDAHFD model revealed abundant dying hepatocytes in the pericentral area accompanied by proliferating hepatocytes in zone 1/2, which resulted in a significant decrease in RFP⁺ pericentral hepatocytes and an increase in RFP⁺ tumours derived from zone 1/2 hepatocytes. Taken together, zone 3 hepatocytes generally possess high neoplastic potential; however, the frequency of zone 3 hepatocyte-derived tumours is dependent on the regeneration pattern of the liver parenchyma in response to liver injury.

We also demonstrated that hepatocytes located in different zones during chronic liver injury exhibit dynamic plasticity. In the MUP + HFD model, RFP⁺ zone 3 hepatocytes supplied new zone 1 hepatocytes to the area immediately adjacent to the portal vein, and these cells were functionally transdifferentiated. Conversely, some pericentral areas were replaced with RFP⁺ hepatocytes that were derived from zone 1/2 hepatocytes but expressed zone 3 markers. Such a dynamic bidirectional plasticity of hepatocytes has not yet been demonstrated. Furthermore, we found that Axin2-expressing hepatocytes subjected to chronic liver injury dramatically expanded to both the pericentral and periportal regions where they were the source of most liver tumours; this suggests that activation of Wnt/β-catenin signalling plays an important role in liver regeneration, and in hepatocarcinogenesis during chronic liver injury.

We assessed whether the metabolic phenotypes of PV- and PP-type HCC are derived from the spatial origin of the tumours or acquired during tumorigenesis and found that the metabolic phenotype was acquired during tumorigenesis. Additionally, these results suggest that the mutational landscape of HCC may not be affected by their spatial origin. However, further studies are required to determine if the same applies to PV-type HCC, as PV-type tumours were rarely found within our mouse models.

A limitation to our study is that we marked only zone 3 hepatocytes during fate tracing, and the behaviour of zone 1/2 hepatocytes was evaluated indirectly by observing RFP⁺ hepatocytes. Not all zone 3 hepatocytes were labelled in *Axin2;tdTomato* mice, as shown by the incomplete recombination of RFP in CYP2E1-expressing hepatocytes in 3-week-old *Axin2;tdTomato* mice. Therefore, we cannot exclude the possibility that some RFP⁺ tumours were derived from unlabelled zone 3 hepatocytes, suggesting that the neoplastic potential of zone 3 hepatocytes may have been underestimated. To complement our findings, cell fate tracing using zone 1 hepatocyte-specific markers should be performed. In addition, we administered TAM to mice early after birth, which might affect the behaviour and carcinogenic potential of zone 3 hepatocytes. Furthermore, the Cre^{ERT2} gene is knocked into the *Axin2* locus in *Axin2-Cre^{ERT2}* mice,²⁸ which causes heterozygous deletion of *Axin2*. Wei *et al.*¹³ showed that increased proliferation of pericentral hepatocytes previously reported by Wang *et al.*⁸ was caused by the heterozygous deletion of *Axin2*. However, DEN-induced HCC development was comparable with that in *Axin2-Cre^{ERT2}* and *Cre^{ERT2}*-negative control mice in the present study (Fig. S5), suggesting that the heterozygous deletion of *Axin2* was unlikely to have affected liver tumorigenesis. Recently, a new *Axin2* bacterial artificial chromosome-transgenic mouse line was developed, in which the endogenous *Axin2* gene was conserved;⁹ further analysis using that mouse line or others could address the above issue.

To summarise, we found that zone 3 hepatocytes generally have high neoplastic potential, and this was attributed, at least in

part, to constitutive activation of Wnt/ β -catenin signalling in the pericentral area. However, the spatial origin of the liver tumour varied depending on the regeneration pattern of the liver parenchyma in response to liver injury. Notably, Axin2-expressing

hepatocytes subjected to chronic liver injury significantly contributed to liver regeneration and possessed high neoplastic potential. Thus, Wnt/ β -catenin signalling is a potential drug target for the prevention of HCC.

Abbreviations

CDAHFD, choline-deficient l-amino acid-defined, high-fat diet; CPS1, carbamoyl phosphate synthetase 1; CYP2E1, cytochrome P450 subfamily 2E1; DEN, diethylnitrosamine; GS, glutamine synthetase; HAL, histidine ammonia lyase; HCC, hepatocellular carcinoma; HFD, high-fat diet; IF, immunofluorescence; ISH, in situ hybridisation; MAFLD, metabolic dysfunction-associated fatty liver disease; MUP, major urinary protein; ND, normal diet; PIK3CA^{Tg}, hepatocyte-specific transgenic mice harbouring mutant PIK3CA variant; PP, periportal; PV, perivenous; RFP, red fluorescent protein; TAM, tamoxifen; TUNEL, terminal deoxynucleotidyl transferase-mediated deoxyuridine triphosphate nick-end labelling; WT, wild-type.

Financial support

This research was supported by Bristol-Myers Squibb Research Grant, Takeda Science Foundation, MSD Life Science Foundation, The Naito Foundation, Life Science Foundation of Japan, The Cell Science Research Foundation, The Mitsubishi Foundation, The Fugaku Foundation, KAKENHI Grant Number 18K07994, AMED under Grant Numbers JP19fk0210059, JP20fk0210059, JP18fk0210040, JP19fk0210040, JP20fk0210040, and JP21fk0210090.

Conflicts of interest

The authors declare no competing interests.

Please refer to the accompanying ICMJE disclosure forms for further details.

Authors' contributions

Performed the experiments, analysed the data, and wrote the paper: SK, YH. Conceived and designed study and wrote the paper: HN. Helped some experiments and interpretation of data and edited the manuscript: SK, YM, TY, KU, YH, NS, MH, MT, HK. Provided critical materials: YT, TN. Edited the manuscript with important intellectual input: YH, KT. Supervised the entire project: KK

Data availability statement

The data generated and/or analysed during the current study are included in this published article (and its [Supplementary data](#)) or available from the corresponding author on reasonable request.

Supplementary data

Supplementary data to this article can be found online at <https://doi.org/10.1016/j.jhepr.2021.100315>.

References

Author names in bold designate shared co-first authorship

- [1] Kietzmann T. Metabolic zonation of the liver: the oxygen gradient revisited. *Redox Biol* 2017;11:622–630.
- [2] Torre C, Perret C, Colnot S. Molecular determinants of liver zonation. *Prog Mol Biol Transl Sci* 2010;97:127–150.
- [3] Rocha AS, Vidal V, Mertz M, Kendall TJ, Charlet A, Okamoto H, et al. The angiocrine factor Rspondin3 is a key determinant of liver zonation. *Cell Rep* 2015;13:1757–1764.
- [4] Halpern KB, Shenhav R, Matcovitch-Natan O, Toth B, Lemze D, Golan M, et al. Single-cell spatial reconstruction reveals global division of labour in the mammalian liver. *Nature* 2017;542:352–356.
- [5] Gougelet A, Torre C, Veber P, Sartor C, Bachelot L, Denechaud PD, et al. T-cell factor 4 and β -catenin chromatin occupancies pattern zonal liver metabolism in mice. *Hepatology* 2014;59:2344–2357.
- [6] Planas-Paz L, Orsini V, Boulter L, Calabrese D, Pikiolek M, Nigsch F, et al. The RSPO-LGR4/5-ZNRF3/RNF43 module controls liver zonation and size. *Nat Cell Biol* 2016;18:467–479.
- [7] Russell JO, Monga SP. Wnt/ β -catenin signaling in liver development, homeostasis, and pathobiology. *Annu Rev Pathol* 2018;13:351–378.
- [8] Wang B, Zhao L, Fish M, Logan CY, Nusse R. Self-renewing diploid Axin2(+) cells fuel homeostatic renewal of the liver. *Nature* 2015;524:180–185.
- [9] Sun T, Pikiolek M, Orsini V, Bergling S, Holwerda S, Morelli L, et al. AXIN2⁺ pericentral hepatocytes have limited contributions to liver homeostasis and regeneration. *Cell Stem Cell* 2020;26:97–107.e106.
- [10] Matsumoto T, Wakefield L, Tarlow BD, Grompe M. In vivo lineage tracing of polyploid hepatocytes reveals extensive proliferation during liver regeneration. *Cell Stem Cell* 2020;26:34–47.e33.
- [11] Chen F, Jimenez RJ, Sharma K, Luu HY, Hsu BY, Ravindranathan A, et al. Broad distribution of hepatocyte proliferation in liver homeostasis and regeneration. *Cell stem cell* 2020;26:27–33.e24.
- [12] Lin S, Nascimento EM, Gajera CR, Chen L, Neuhöfer P, Garbuzov A, et al. Distributed hepatocytes expressing telomerase repopulate the liver in homeostasis and injury. *Nature* 2018;556:244–248.
- [13] Wei Y, Wang YG, Jia Y, Li L, Yoon J, Zhang S, et al. Liver homeostasis is maintained by midlobular zone 2 hepatocytes. *Science* 2021;371:eabb1625.
- [14] He L, Pu W, Liu X, Zhang Z, Han M, Li Y, et al. Proliferation tracing reveals regional hepatocyte generation in liver homeostasis and repair. *Science* 2021;371:eabc4346.
- [15] Nakagawa H, Maeda S. Inflammation- and stress-related signaling pathways in hepatocarcinogenesis. *World J Gastroenterol* 2012;18:4071–4081.
- [16] Eslam M, Sanyal AJ, George J, International Consensus Panel. MAFLD: a consensus-driven proposed nomenclature for metabolic associated fatty liver disease. *Gastroenterology* 2020;158:1999–2014.e1991.
- [17] Mu X, Español-Suñer R, Mederacke I, Affò S, Manco R, Sempoux C, et al. Hepatocellular carcinoma originates from hepatocytes and not from the progenitor/biliary compartment. *J Clin Invest* 2015;125:3891–3903.
- [18] Jörs S, Jeliázkova P, Ringelhan M, Thalhammer J, Dürfl S, Ferrer J, et al. Lineage fate of ductular reactions in liver injury and carcinogenesis. *J Clin Invest* 2015;125:2445–2457.
- [19] Font-Burgada J, Shalapour S, Ramaswamy S, Hsueh B, Rossell D, Umemura A, et al. Hybrid periportal hepatocytes regenerate the injured liver without giving rise to cancer. *Cell* 2015;162:766–779.
- [20] Zucman-Rossi J, Villanueva A, Nault JC, Llovet JM. Genetic landscape and biomarkers of hepatocellular carcinoma. *Gastroenterology* 2015;149:1226–1239.e1224.
- [21] Dhar D, Antonucci L, Nakagawa H, Kim JY, Glitzner E, Caruso S, et al. Liver cancer initiation requires p53 inhibition by CD44-enhanced growth factor signaling. *Cancer Cell* 2018;33:1061–1077.e1066.
- [22] Ipsen DH, Lykkesfeldt J, Tveden-Nyborg P. Molecular mechanisms of hepatic lipid accumulation in non-alcoholic fatty liver disease. *Cellular and molecular life sciences. Cell Mol Life Sci* 2018;75:3313–3327.
- [23] Nakagawa H, Umemura A, Taniguchi K, Font-Burgada J, Dhar D, Ogata H, et al. ER stress cooperates with hypernutrition to trigger TNF-dependent spontaneous HCC development. *Cancer Cell* 2014;26:331–343.
- [24] Kudo Y, Tanaka Y, Tateishi K, Yamamoto K, Yamamoto S, Mohri D, et al. Altered composition of fatty acids exacerbates hepatotumorigenesis during activation of the phosphatidylinositol 3-kinase pathway. *J Hepatol* 2011;55:1400–1408.
- [25] Fujiwara N, Nakagawa H, Enooku K, Kudo Y, Hayata Y, Nakatsuka T, et al. CPT2 downregulation adapts HCC to lipid-rich environment and promotes carcinogenesis via acylcarnitine accumulation in obesity. *Gut* 2018;67:1493–1504.
- [26] Hayata Y, Nakagawa H, Kurosaki S, Kawamura S, Matsushita Y, Hayakawa Y, et al. Axin2⁺ peribiliary glands in the periampullary region generate biliary epithelial stem cells that give rise to ampullary carcinoma. *Gastroenterology* 2021;160:2133–2148.e6.
- [27] Apte U, Zeng G, Thompson MD, Muller P, Micsenyi A, Cieply B, et al. β -Catenin is critical for early postnatal liver growth. *Am J Physiol Gastrointest Liver Physiol* 2007;292:G1578–G1585.

- [28] van Amerongen R, Bowman AN, Nusse R. Developmental stage and time dictate the fate of Wnt/ β -catenin-responsive stem cells in the mammary gland. *Cell Stem Cell* 2012;11:387–400.
- [29] Désert R, Rohart F, Canal F, Sicard M, Desille M, Renaud S, et al. Human hepatocellular carcinomas with a periportal phenotype have the lowest potential for early recurrence after curative resection. *Hepatology* 2017;66:1502–1518.
- [30] Maeda S, Kamata H, Luo JL, Leffert H, Karin M. IKK β couples hepatocyte death to cytokine-driven compensatory proliferation that promotes chemical hepatocarcinogenesis. *Cell* 2005;121:977–990.
- [31] Park EJ, Lee JH, Yu GY, He G, Ali SR, Holzer RG, et al. Dietary and genetic obesity promote liver inflammation and tumorigenesis by enhancing IL-6 and TNF expression. *Cell* 2010;140:197–208.
- [32] Ikawa-Yoshida A, Matsuo S, Kato A, Ohmori Y, Higashida A, Kaneko E, et al. Hepatocellular carcinoma in a mouse model fed a choline-deficient, L-amino acid-defined, high-fat diet. *Int J Exp Pathol* 2017;98:221–233.
- [33] Nakagawa H. Recent advances in mouse models of obesity- and nonalcoholic steatohepatitis-associated hepatocarcinogenesis. *World J Hepatol* 2015;7:2110–2118.
- [34] Kang JS, Wanibuchi H, Morimura K, Gonzalez FJ, Fukushima S. Role of CYP2E1 in diethylnitrosamine-induced hepatocarcinogenesis in vivo. *Cancer Res* 2007;67:11141–11146.
- [35] Devereux TR, Anna CH, Foley JF, White CM, Sills RC, Barrett JC. Mutation of beta-catenin is an early event in chemically induced mouse hepatocellular carcinogenesis. *Oncogene* 1999;18:4726–4733.
- [36] Yamashita T, Ji J, Budhu A, Forgues M, Yang W, Wang HY, et al. EpCAM-positive hepatocellular carcinoma cells are tumor-initiating cells with stem/progenitor cell features. *Gastroenterology* 2009;136:1012–1024.
- [37] Dow M, Pyke RM, Tsui BY, Alexandrov LB, Nakagawa H, Taniguchi K, et al. Integrative genomic analysis of mouse and human hepatocellular carcinoma. *Proc Natl Acad Sci U S A* 2018;115:E9879–E9888.
- [38] Weglarz TC, Degen JL, Sandgren EP. Hepatocyte transplantation into diseased mouse liver. Kinetics of parenchymal repopulation and identification of the proliferative capacity of tetraploid and octaploid hepatocytes. *Am J Pathol* 2000;157:1963–1974.
- [39] Ang CH, Hsu SH, Guo F, Tan CT, Yu VC, Visvader JE, et al. Lgr5⁺ pericentral hepatocytes are self-maintained in normal liver regeneration and susceptible to hepatocarcinogenesis. *Proc Natl Acad Sci U S A* 2019;116:19530–19540.